Radical Frameworks

International Edition: DOI: 10.1002/anie.201501706
German Edition: DOI: 10.1002/ange.201501706

Radical Covalent Organic Frameworks: A General Strategy to Immobilize Open-Accessible Polyradicals for High-Performance Capacitive Energy Storage**

*Fei Xu, Hong Xu, Xiong Chen, Dingcai Wu, Yang Wu, Hao Liu, Cheng Gu, Ruowen Fu, and Donglin Jiang**

Abstract: *Ordered π-columns and open nanochannels found in covalent organic frameworks (COFs) could render them able to store electric energy. However, the synthetic difficulty in achieving redox-active skeletons has thus far restricted their potential for energy storage. A general strategy is presented for converting a conventional COF into an outstanding platform for energy storage through post-synthetic functionalization with organic radicals. The radical frameworks with openly accessible polyradicals immobilized on the pore walls undergo rapid and reversible redox reactions, leading to capacitive energy storage with high capacitance, high-rate kinetics, and robust cycle stability. The results suggest that channel-wall functional engineering with redox-active species will be a facile and versatile strategy to explore COFs for energy storage.*

Covalent organic frameworks (COFs) are an emerging class of crystalline porous polymers with highly ordered organic building blocks and discrete nanopores.[1–21] The latticed π-columns and one-dimensional open nanochannels render them able to store electric energy. However, COFs capable of electrochemical energy storage can be currently synthesized through only a few skeletons, limiting the access to and exploration of new structures and functions.[17,18] In this context, a new and general strategy that avoids such synthetic limitations and allows for the conversion of a conventional COF into electrochemically active skeletons is highly desirable.

[*] F. Xu, H. Xu, X. Chen, Y. Wu, Dr. C. Gu, Prof. Dr. D. Jiang
Department of Materials Molecular Science
Institute for Molecular Science
National Institutes of Natural Sciences
5-1 Higashiyama, Myodaiji, Okazaki 444-8787 (Japan)
E-mail: jiang@ims.ac.jp
F. Xu, Prof. Dr. D. Wu, H. Liu, Prof. Dr. R. Fu
Materials Science Institute
School of Chemistry and Chemical Engineering
Sun Yat-sen University, Guangzhou, 510275 (P. R. China)

[**] This work was supported by a Grant-in-Aid for Scientific Research (A) (24245030) from MEXT of Japan. R.F. thanks the National Key Basic Research Program of China (973, 2014CB932402) and the NSFC (51232005). D.W. thanks the National Science Foundation for Excellent Young Scholars (No. 51422307), the NSFC (51372280 and 51173213), and the Guangdong Natural Science Funds for Distinguished Young Scholars project (S2013050014408).

Supporting information for this article is available on the WWW under http://dx.doi.org/10.1002/anie.201501706.

Organic radicals have received considerable attentions because their unpaired electrons endow the materials with unusual electronic, magnetic, optical, and redox properties.[22–25] In this study, we developed a facile and general strategy that converts a conventional COF into an outstanding redox-active platform for energy storage by post-synthetic channel-wall functionalization with organic radicals. With this achievement, we show a new platform based on radical COFs for energy storage. We demonstrated this strategy using a conventional imine-linked COF (Figure 1a, $[HC{\equiv}C]_{X\%}$-NiP-COF; $X = 0$, 50, and 100) as a scaffold with nickel porphyrin at the vertices and ethynyl units on the channel walls; this COF is electrochemically inactive. Reaction of 2,5-bis(2-propynyloxy)terephthalaldehyde (BPTA) and 2,5-dimethoxyterephthalaldehyde (DMTA) at different molar ratios with nickel 5,10,15,20-tetrakis(4′-tetraphenylamino) porphyrin (NiP) under solvothermal conditions yielded NiP-COF, $[HC{\equiv}C]_{50\%}$-NiP-COF COFs, and $[HC{\equiv}C]_{100\%}$-NiP-COF with 0%, 50%, and 100% ethynyl units on the COF walls (Figure 1a).[6] The ethynyl groups undergo click reaction with 4-azido-2,2,6,6-tetramethyl-1-piperidinyloxy in a smooth and clean manner to yield $[TEMPO]_{50\%}$-NiP-COF and $[TEMPO]_{100\%}$-NiP-COF quantitatively (Figure 1a).

The accomplishment of click reactions was indicated by the disappearance of the vibration bands of the C≡C and CC–H units at 2120 and 3290 cm^{-1} and the appearance of new bands at 2941 and 2980 cm^{-1}, which were assigned to the TEMPO units (Supporting Information, Figure S1). Elemental analysis (Table S1), field emission scanning electron microscopy (Figure S2), high-resolution transmission electron microscopy (Figure S3), X-ray diffraction (XRD), and gas adsorption measurements confirmed the formation of radical COFs. These results indicate that the post-synthetic wall-engineering strategy is useful for converting a conventional COF into radical frameworks in which openly accessible polyradicals are covalently immobilized on the channel walls in a controlled manner. To the best of our knowledge, this is the first example of radical COFs.

NiP-COF, $[HC{\equiv}C]_{50\%}$-NiP-COF, and $[HC{\equiv}C]_{100\%}$-NiP-COF exhibited XRD patterns with diffraction peaks at 3.4°, 7.0°, 7.6°, and 20–24°, which were assigned to the 100, 110, 200, and 001 facets, respectively (Figure 1c).[6] $[TEMPO]_{50\%}$-NiP-COF exhibited a similar XRD pattern with prominent peaks at 3.5°, 7.0°, 7.6°, and 20–24°, which were assigned to the 100, 110, 200, and 001 facets, respectively (blue curve). In contrast, $[TEMPO]_{100\%}$-NiP-COF exhibited quite broadened signals (red curve). This result is reasonable because the

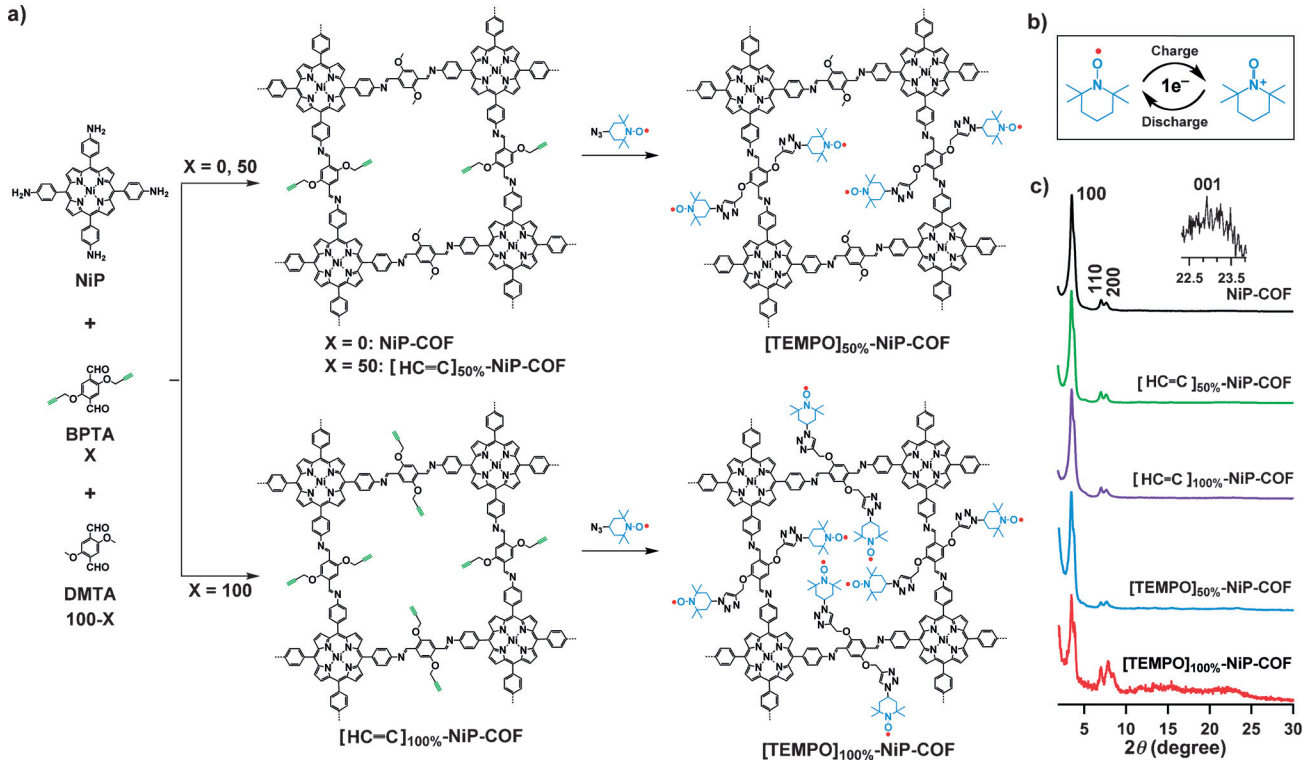

Figure 1. a) Synthesis of radical COFs ([TEMPO]$_{100\%}$-NiP-COF and [TEMPO]$_{50\%}$-NiP-COF) with TEMPO radicals immobilized on the walls by functionalization of [HC≡C]$_{100\%}$-NiP-COF and [HC≡C]$_{50\%}$-NiP-COF. b) The charge–discharge process of TEMPO based on a one-electron redox reaction. c) XRD patterns of the COFs.

presence of large numbers of flexible chains in the pores of COFs weakens the diffractions.[6] These results indicate that the crystalline structure of NiP-COF is retained in the radical COFs.

Nitrogen sorption at 77 K was measured to investigate the porosity. NiP-COF (Figure 2a, black curve), [HC≡C]$_{50\%}$-NiP-COF (green curve), and [HC≡C]$_{100\%}$-NiP-COF (purple curve)

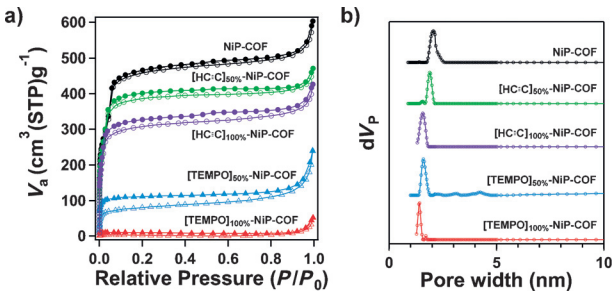

Figure 2. a) Nitrogen sorption isotherm curves (○, △ adsorption, ●, ▲ desorption) and b) pore size distribution profiles of the COFs.

exhibited a large uptake at low pressure ($P/P_0 < 0.1$), which is characteristic of micropores or small nanopores. Their Brunauer–Emmett–Teller (BET) surface areas were evaluated as high as 1447, 1219, and 975 $m^2 g^{-1}$, respectively (Supporting Information, Table S1). Pore size distribution profiles calculated using nonlocal density function theory method confirmed the presence of a single type of pore in these COFs (Figure 2b). The pore size was calculated to be 2.06, 1.88, and 1.63 nm for NiP-COF, [HC≡C]$_{50\%}$-NiP-COF, and [HC≡C]$_{100\%}$-NiP-COF, respectively (Figure 2b; Supporting Information, Table S2). Upon immobilization with the TEMPO units, the resulting [TEMPO]$_{50\%}$-NiP-COF (Figure 2a, blue curve) and [TEMPO]$_{100\%}$-NiP-COF (red curve) had BET surface area of 264 and 5.2 $m^2 g^{-1}$, respectively, whereas their pores size was evaluated to be 1.6 and 1.4 nm, respectively (Figure 2b; Supporting Information, Table S2).

TEMPO is a typical organic radical that not only holds all the unique properties of radicals but also features redox ability for energy storage by reversibly switching between the oxidation states of the neutral radical and the oxoammonium cation (Figure 1b).[22] To investigate the possibility of redox reaction of the radical COFs, we fabricated thin films of [TEMPO]$_{50\%}$-NiP-COF and [TEMPO]$_{100\%}$-NiP-COF by pressing the COF sample (20 wt%), carbon black conductor (70 wt%), and polytetrafluoroethylene binder (PTFE, 10 wt%) onto a platinum mesh current collector. The films contain 1.2 mg of COFs and have a mass of 6 mg.

Cyclic voltammetry (CV) of these [TEMPO]$_{50\%}$-NiP-COF and [TEMPO]$_{100\%}$-NiP-COF films were conducted in a three-electrode cell with platinum plate counter electrode and Ag/Ag$^+$ reference electrode in $(C_4H_9)_4NClO_4$ electrolyte (0.1M) at 25°C. Both [TEMPO]$_{50\%}$-NiP-COF (Figure 3a, blue curve) and [TEMPO]$_{100\%}$-NiP-COF (red curve) exhibited a pair of reversible peaks, which were assigned to one-electron redox reactions of the TEMPO radicals. By contrast,

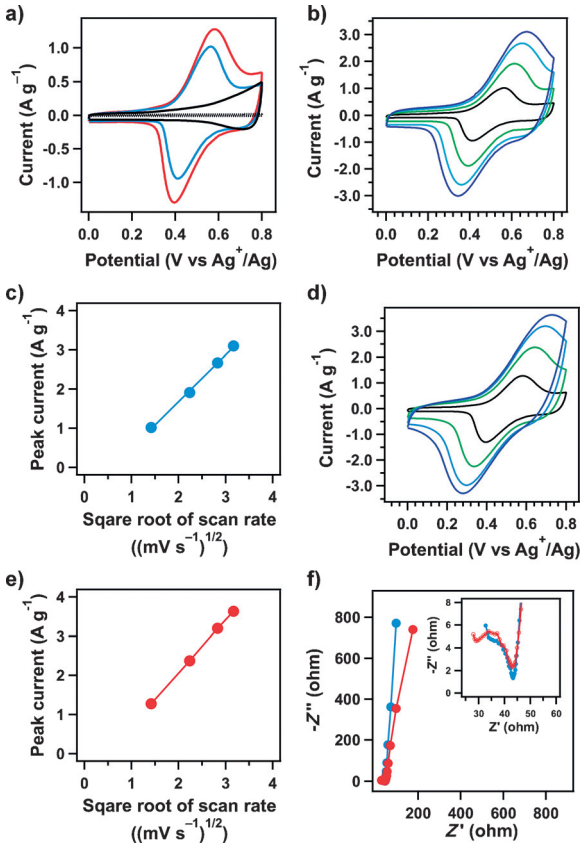

Figure 3. a) CV profiles of $[TEMPO]_{100\%}$-NiP-COF (red curve), $[TEMPO]_{50\%}$-NiP-COF (blue curve), $[Ph]_{100\%}$-NiP-COF (black curve), and a mixture of carbon black and PTFE (dotted curve), in the form of film electrodes. b) CV profiles of $[TEMPO]_{50\%}$-NiP-COF at different sweep rate constants (black curve: 2 mV s^{-1}; green curve: 5 mV s^{-1}; sky-blue curve: 8 mV s^{-1}; blue curve: 10 mV s^{-1}). c) Plot of normalized peak current versus square root of the sweep rate for $[TEMPO]_{50\%}$-NiP-COF. d) CV profiles of $[TEMPO]_{100\%}$-NiP-COF at different sweep rate constants (black curve: 2 mV s^{-1}; green curve: 5 mV s^{-1}; sky-blue curve: 8 mV s^{-1}; blue curve: 10 mV s^{-1}). e) Plot of normalized peak current versus square root of the sweep rate for $[TEMPO]_{100\%}$-NiP-COF. f) Nyquist plots of $[TEMPO]_{100\%}$-NiP-COF (red curve) and $[TEMPO]_{50\%}$-NiP-COF (blue curve) measured from 10 KHz to 10 mHz. Inset: enlarged semicircle profiles in the high-frequency region.

COFs without redox-active TEMPO units, such as $[Ph]_{100\%}$-NiP-COF (black curve, for structure see the Supporting Information, Figure S4) with phenyl groups on the channel walls, did not show such redox peaks. Moreover, the electrode with only carbon black and PTPE (dotted curve) is also not redox-active. These positive effects clearly confirmed the effectiveness of channel-wall functionalization in introducing redox activity. Immobilization of the TEMPO radicals on the COF walls turns the originally inert scaffold into a redox-active skeleton in which the electrochemical process originates from the reversible reduction and oxidation of the TEMPO units.

From the CV profiles (Figure 3a), $[TEMPO]_{100\%}$-NiP-COF (red curve) acquires a larger output current compared to that of $[TEMPO]_{50\%}$-NiP-COF (blue curve). This result suggests that $[TEMPO]_{100\%}$-NiP-COF enables a higher capacitance in energy storage as a result of its dense TEMPO radicals on the walls. By contrast, $[TEMPO]_{50\%}$-NiP-COF allows high-rate electrode kinetics for a quick charge and discharge cycle, as evidenced by its narrower peak separation between the oxidative and reductive waves (155 mV for $[TEMPO]_{50\%}$-NiP-COF and 186 mV for $[TEMPO]_{100\%}$-NiP-COF). A relatively low TEMPO density on the COF walls endows $[TEMPO]_{50\%}$-NiP-COF with a higher surface area and larger pore that benefit the ion transport into and out of the pores of the COFs.

The redox peaks did not alter their positions after multiple scans while keeping the sweep rate constant, indicating the reversibility of the redox processes in these COFs. It should be note that the TEMPO radicals are covalently immobilized on the channel walls of COFs and do not dissolve in the electrolyte. In the case of such dissolving event, the current peak is expected to decrease steadily and the materials eventually lose their energy-storage capability. A high insolubility of the electrochemically active species is fundamentally important for their use in electrochemical devices. Furthermore, the peak positions did not change significantly at sweep rate over a wide range, indicating that a fast and reversible electron transfer occurs in the TEMPO groups (Figure 3b,d). A plot of normalized peak current versus the square root of the scan rate shows a linear relationship (Figure 3c,e). According to the Randles–Sevcik equation,[26] this linear plot yields a diffusion coefficient of active species to be 10^{-10} cm^{2}s^{-1} in these COF pores.

Electrochemical impedance spectroscopy (EIS) was further conducted to corroborate the electrolyte ion transport ability. $[TEMPO]_{100\%}$-NiP-COF (Figure 3f, red curve) and $[TEMPO]_{50\%}$-NiP-COF (blue curve) both present a single and similar semicircle in the high frequency region (Figure 3d, inset), indicating a similar resistance owing to the same COF scaffold. The linear curve at low frequencies implies a capacitive behavior, whereas the line slope reflects the ion diffusion process. $[TEMPO]_{50\%}$-NiP-COF exhibited an almost vertical curve, which is typical for an electrode material that enables ideal ion transport in the pores.

Based on these results, we conducted galvanostatic charge and discharge tests to evaluate the energy-storage properties. $[TEMPO]_{50\%}$-NiP-COF and $[TEMPO]_{100\%}$-NiP-COF exhibited voltage plateaus at a same potential of 0.5 V versus Ag/Ag$^+$ (Figure 4a,b, red curves), which indicates the electron transfer to or from the TEMPO units. These capacitive energy storage based on the redox reaction of the TEMPO units is consistent with the CV profiles. One significant feature is that the voltage plateaus retained at 0.5 V irrespective of the current density, indicating extremely high reversibility of the redox reaction for energy storage throughout the charge and discharge processes.

Figure 4c presents the capacitance of these radical COFs calculated from discharge curves. $[TEMPO]_{50\%}$-NiP-COF and $[TEMPO]_{100\%}$-NiP-COF are high-performance materials for energy storage and exhibit high capacitances over a wide range of current densities spanning from 100 to 2000 mA g^{-1}. $[TEMPO]_{100\%}$-NiP-COF exhibited higher capacitances compared to those of $[TEMPO]_{50\%}$-NiP-COF. For example, at a current density of 100 mA g^{-1}, $[TEMPO]_{100\%}$-NiP-COF and $[TEMPO]_{50\%}$-NiP-COF exhibited a capacitance of 167 and

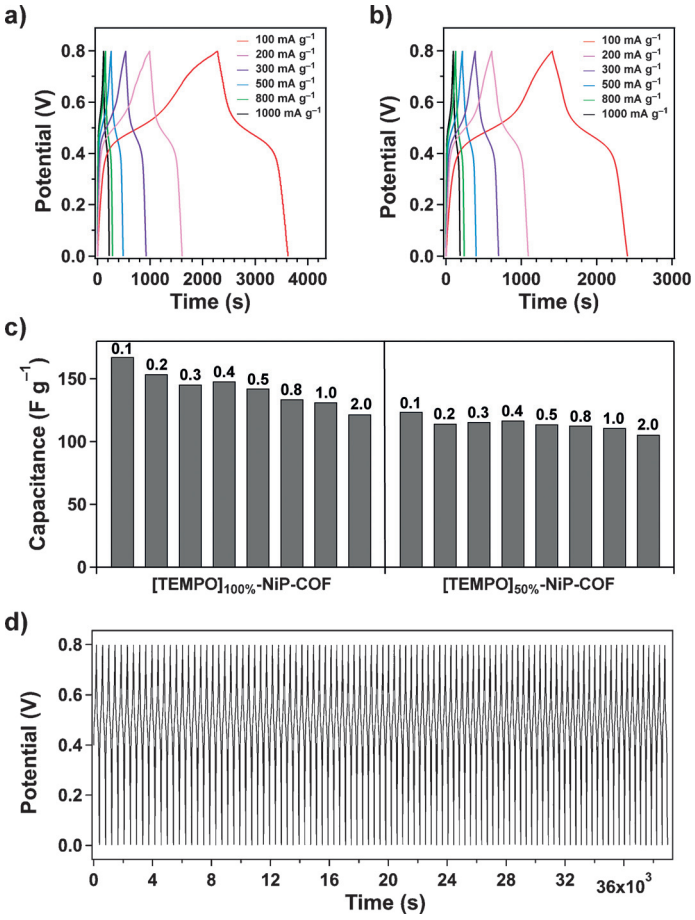

Figure 4. Charge and discharge curves of a) $[TEMPO]_{100\%}$-NiP-COF and b) $[TEMPO]_{50\%}$-NiP-COF at different current densities. c) Capacitance of $[TEMPO]_{100\%}$-NiP-COF and $[TEMPO]_{50\%}$-NiP-COF at different current densities (numbers on the top of the bars are the current density in $A\,g^{-1}$). d) Charge and discharge stability of $[TEMPO]_{50\%}$-NiP-COF over 100 cycles at a current density of 500 $mA\,g^{-1}$.

$124\,F\,g^{-1}$, respectively. $[TEMPO]_{100\%}$-NiP-COF still works well to exhibit a capacitance of as high as $113\,F\,g^{-1}$ as the current density was increased to $2000\,mA\,g^{-1}$. Remarkably, $[TEMPO]_{50\%}$-NiP-COF at $2000\,mA\,g^{-1}$ retained a capacitance of $101\,F\,g^{-1}$, which is as high as 81% of the capacitance at $100\,mA\,g^{-1}$. Figure S5 shows that $[TEMPO]_{50\%}$-NiP-COF has a high retention in capacitance compared to $[TEMPO]_{100\%}$-NiP-COF. This result is likely related to the high porosity of $[TEMPO]_{50\%}$-NiP-COF that allows for high-rate ion transport as also revealed by CV and EIS. The radical COFs exhibited higher or similar capacitance as those of metal ion-based redox active MOFs[27–30] and is much higher than that of redox-active DAAQ-TFP COFs ($40\,F\,g^{-1}$).[18] Recently, MOFs and COFs have shown enhanced utilization of redxo-active units by decreasing the thickness of films to even nanometer that improves the accessibility of redox-active units.[31,32]

Cycle stability of electrochemical active species is crucial for applications. Most pseudocapacitive electrodes based on organic materials or inorganic metal oxides reported to date for capacitive energy storage are problematic in cycle stability.[31,33–35] By contrast, the covalently immobilized TEMPO radicals on the channel walls are insoluble and exhibit outstanding cycle performance. Figure 4d presents the result of cycle tests using $[TEMPO]_{50\%}$-NiP-COF at $500\,mA\,g^{-1}$. The charge-discharge curves retain their shapes and the capacitance is constant upon even 100 cycles (Figure 4d; for an enlarged profile, see the Supporting Information, Figure S6).

To the best of our knowledge, this is the first example of radical porous materials for electrochemical energy storage.[18] In crystalline porous radical COFs, the organic radicals are covalently immobilized to assure an outstanding structural stability, whereas the ordered pores promote ion transport, and the high surface area offers a large interface for the access to redox-active sites. These positive structural effects make radical COFs an attractive material for energy storage. For the COF systems, to reduce the inactive part of the framework may provide a promising way to enhance volume charge density. We envisage that this strategy is possible by designing a full use of the substitution of edge units, multiple numbers of radical units appended to the substitution chain, and large hexagonal COF skeletons.

In summary, we have developed a facile and general strategy that enables the conversion of a conventional COF into an outstanding redox-active energetic framework by channel-wall functionalization. The high-throughput click reaction is useful for creating polyradical-immobilized channel walls while retaining crystallinity and accessibility. Our results reveal the enormous potential of COFs as an appealing platform for construction of electrode materials for energy storage, a newly developed function of COFs worthy of further exploration. Given the limited chemical reactions that allow the direct synthesis of electrochemically active skeletons, together with the availability of a broad diversity of redox-active groups for functionalization, we anticipate that the present post-synthetic channel-wall engineering strategy will be critical to exploring COF materials for high-performance energy storage and power supply.

Keywords: capacitors · covalent organic frameworks · energy storage · radicals · synthesis

How to cite: *Angew. Chem. Int. Ed.* **2015**, *54*, 6814–6818
Angew. Chem. **2015**, *127*, 6918–6922

[1] X. Feng, X. S. Ding, D. Jiang, *Chem. Soc. Rev.* **2012**, *41*, 6010–6022.
[2] M. Dogru, T. Bein, *Chem. Commun.* **2014**, *50*, 5531–5546.
[3] X. Feng, L. Liu, Y. Honsho, A. Saeki, S. Seki, S. Irle, Y. Dong, A. Nagai, D. Jiang, *Angew. Chem. Int. Ed.* **2012**, *51*, 2618–2622; *Angew. Chem.* **2012**, *124*, 2672–2676.
[4] Z. Li, X. Feng, Y. Zou, Y. Zhang, H. Xia, X. Liu, Y. Mu, *Chem. Commun.* **2014**, *50*, 13825–13828.
[5] A. Nagai, Z. Guo, X. Feng, S. Jin, X. Chen, X. Ding, D. Jiang, *Nat. Commun.* **2011**, DOI: 10.1038/ncomms1542.
[6] H. Xu, X. Chen, J. Gao, J. Lin, M. Addicoat, S. Irle, D. Jiang, *Chem. Commun.* **2014**, *50*, 1292–1294.
[7] L. Stegbauer, K. Schwinghammer, B. V. Lotsch, *Chem. Sci.* **2014**, *5*, 2789–2793.

[8] S. Kandambeth, D. B. Shinde, M. K. Panda, B. Lukose, T. Heine, R. Banerjee, *Angew. Chem. Int. Ed.* **2013**, *52*, 13052 – 13056; *Angew. Chem.* **2013**, *125*, 13290 – 13294.
[9] H. Furukawa, O. M. Yaghi, *J. Am. Chem. Soc.* **2009**, *131*, 8875 – 8883.
[10] C. J. Doonan, D. J. Tranchemontagne, T. G. Glover, J. R. Hunt, O. M. Yaghi, *Nat. Chem.* **2010**, *2*, 235 – 238.
[11] S. Chandra, S. Kandambeth, B. P. Biswal, B. Lukose, S. M. Kunjir, M. Chaudhary, R. Babarao, T. Heine, R. Banerjee, *J. Am. Chem. Soc.* **2013**, *135*, 17853 – 17861.
[12] Q. Fang, Z. Zhuang, S. Gu, R. B. Kaspar, J. Zheng, J. Wang, S. Qiu, Y. Yan, *Nat. Commun.* **2014**, *5*, 4503.
[13] D. N. Bunck, W. R. Dichtel, *Angew. Chem. Int. Ed.* **2012**, *51*, 1885 – 1889; *Angew. Chem.* **2012**, *124*, 1921 – 1925.
[14] D. N. Bunck, W. R. Dichtel, *Chem. Commun.* **2013**, *49*, 2457 – 2459.
[15] Z. Kahveci, T. Islamoglu, G. A. Shar, R. Ding, H. M. El-Kaderi, *CrystEngComm* **2013**, *15*, 1524 – 1527.
[16] M. G. Rabbani, A. K. Sekizkardes, Z. Kahveci, T. E. Reich, R. Ding, H. M. El-Kaderi, *Chem. Eur. J.* **2013**, *19*, 3324 – 3328.
[17] F. Xu, S. Jin, H. Zhong, D. C. Wu, X. Yang, X. Chen, H. Wei, R. W. Fu, D. Jiang, *Sci. Rep.* **2015**, *5*, 8225, DOI: 10.1038/srep08225.
[18] C. R. DeBlase, K. E. Silberstein, T. T. Truong, H. D. Abruna, W. R. Dichtel, *J. Am. Chem. Soc.* **2013**, *135*, 16821 – 16824.
[19] G. H. V. Bertrand, V. K. Michaelis, T. Ong, R. G. Griffin, M. Dincă, *Proc. Natl. Acad. Sci. USA* **2013**, *110*, 4923 – 4928.
[20] M. Calik, F. Auras, L. M. Salonen, K. Bader, I. Grill, M. Handloser, D. D. Medina, M. Dogru, F. Lobermann, D. Trauner, A. Hartschuh, T. Bein, *J. Am. Chem. Soc.* **2014**, *136*, 17802 – 17807.
[21] S. Chandra, T. Kundu, S. Kandambeth, R. BabaRao, Y. Marathe, S. M. Kunjir, R. Banerjee, *J. Am. Chem. Soc.* **2014**, *136*, 6570 – 6573.
[22] M. Mas-Torrent, N. Crivillers, C. Rovira, J. Veciana, *Chem. Rev.* **2012**, *112*, 2506 – 2527.
[23] T. B. Faust, D. M. D'Alessandro, *RSC Adv.* **2014**, *4*, 17498 – 17512.
[24] L. C. Li, R. Matsuda, I. Tanaka, H. Sato, P. Kanoo, H. J. Jeon, M. L. Foo, A. Wakamiya, Y. Murata, S. Kitagawa, *J. Am. Chem. Soc.* **2014**, *136*, 7543 – 7546.
[25] S. V. Potts, L. J. Barbour, D. A. Haynes, J. M. Rawson, G. O. Lloyd, *J. Am. Chem. Soc.* **2011**, *133*, 12948 – 12951.
[26] P. Zanello, *Inorganic Electrochemistry: Theory, Practice and Application*, The Royal Society of Chemistry, London, **2003**.
[27] R. Díaz, M. G. Orcajo, J. A. Botas, G. Calleja, J. Palma, *Mater. Lett.* **2012**, *68*, 126 – 128.
[28] S. L. Li, Q. Xu, *Energy Environ. Sci.* **2013**, *6*, 1656 – 1683.
[29] D. Y. Lee, S. J. Yoon, N. K. Shrestha, S. H. Lee, H. Ahn, S. H. Han, *Microporous Mesoporous Mater.* **2012**, *153*, 163 – 165.
[30] Y. L. Gao, J. X. Wu, W. Zhang, Y. Y. Tan, J. Gao, J. C. Zhao, B. H. J. Tang, *New J. Chem.* **2015**, *39*, 94 – 97.
[31] K. M. Choi, H. M. Jeong, J. H. Park, Y. B. Zhang, J. K. Kang, O. M. Yaghi, *ACS Nano* **2014**, *8*, 7451 – 7457.
[32] C. R. DeBlase, K. Hernández-Burgos, K. E. Silberstein, G. G. Rodríguez-Calero, R. P. Bisbey, H. D. Abruña, W. R. Dichtel, *ACS Nano* **2015**, *9*, 3178 – 3183.
[33] P. Simon, Y. Gogotsi, *Nat. Mater.* **2008**, *7*, 845 – 854.
[34] I. Kovalenko, D. G. Bucknall, G. Yushin, *Adv. Funct. Mater.* **2010**, *20*, 3979 – 3986.
[35] G. P. Wang, L. Zhang, J. J. Zhang, *Chem. Soc. Rev.* **2012**, *41*, 797 – 828.

Received: February 23, 2015
Revised: March 21, 2015
Published online: April 23, 2015

